J. Fluid Mech. (1982), *vol.* 116, *pp.* 207–225
Printed in Great Britain

Long-time evolution of an unstable water-wave train

By MICHAEL STIASSNIE AND URI I. KROSZYNSKI

Department of Civil Engineering and Coastal & Marine Engineering Research Institute, Technion, I.I.T., Technion City, Haifa 32000, Israel

(Received 2 March 1981)

The long-time evolution of an unstable wave train, consisting of a carrier wave and two 'side-band' components, is investigated analytically. Mathematical expressions, involving Jacobian elliptic functions, for the wave envelope characteristics are derived. The solution yields the dependence of the long-time evolution on the initial disturbance. Of special interest is the simple formula for the modulation–demodulation recurrence period. The latter is shown to yield results in good agreement with those obtained from numerical solutions of the nonlinear Schrödinger equation.

1. Introduction

1.1. *General*

One of the remarkable properties of weakly nonlinear dispersive systems is the existence of steady, continuous, progressive wave trains of finite amplitude, the permanent form of which results from the balance between dispersion and nonlinear effects. Concerning gravity waves on water of uniform depth, the search for mathematical solutions of such nature has been the subject of many investigations since the classical work of Stokes (1849). The stability of a train of steady, periodic water waves was taken for granted until quite recently. Thus the discovery by Benjamin & Feir (1967) that weakly nonlinear water wave trains are unstable to modulation perturbations aroused considerable interest. The problem was to predict their subsequent behaviour in time, i.e. their long-time evolution.

Wave-flume experiments by Lake *et al.* (1977) have shown how the unstable modulations grow in time, reach a maximum and then subside. Furthermore, the experiments have shown how the unsteady wave train becomes, at some stage of its evolution, nearly uniform again. This interesting behaviour was also confirmed by numerical computations (carried out by the same authors) using the nonlinear Schrödinger (NLS) equation, derived for water of finite depth by Hasimoto & Ono (1972), which proved to represent satisfactorily the long-time evolution of conservative water-wave trains.

Thus, in the absence of dissipation, there is no permanent end state, but an unsteady series of modulation and demodulation cycles, known as the Fermi–Pasta–Ulam recurrence phenomenon. The cyclic evolution of unsteady wave trains, through their influence on the mean water level and on the average currents, introduces new length and time scales, which are one or two orders of magnitude larger than the length and period of the carrier wave, respectively. A quantitative estimate of these additional scales is of great practical interest, since they are probably related to such phenomena as surf beats (Longuet-Higgins & Stewart 1962), longshore cellular structure, and harbour resonance.

Almost all previous theoretical research on the long-time evolution of continuous wave trains has relied upon numerical solutions; for instance the work by Yuen & Ferguson (1978) on the influence of initial conditions on the long-time evolution, or the work by Martin & Yuen (1980), where numerical results for the spread of energy during this evolution are computed. Considering the limitation to particular cases inherent in numerical investigations, we have chosen to present an analytical approach (§2) which, though approximate, allows for a general analysis of the solution. The range of applicability of this approach is also determined. In §3, results from the analytical approach are compared to those of a reference solution, showing the validity of the behaviour predicted by the former as well as its limitations. In §4, a few conclusions of considerable physical significance are drawn from the relatively simple expressions obtained.

1.2. *Mathematical statement of the problem*

We consider a system in one horizontal dimension, initially composed of a carrier wave of amplitude a and wavenumber k and a symmetric 'side-band' disturbance, consisting of a pair of identical progressive waves of very small amplitude β and wave numbers $k \pm \Delta k$ differing slightly from that of the carrier, where $\Delta k/k = \gamma ak$ is taken as being proportional to the (also small) carrier steepness.

The initial water-surface elevation for such a system is given by

$$\eta(x,0) = a\mathscr{R}\{e^{ikx} + \beta \exp i[(1+\gamma ak)\,kx + \alpha] + \beta \exp i[(1-\gamma ak)\,kx + \alpha]\}. \quad (1.1)$$

In (1.1) x is the horizontal distance and α a phase shift, also considered identical for both side-band disturbance components. The dimensionless parameters γ and α are assumed to be $O(1)$, while the perturbation energy, proportional to $\epsilon = 2\beta^2$, is much smaller. It is the aim of this paper to study the evolution in time of such a system, as governed by the laws of gravity wave propagation in water.

For water of uniform depth h, the following relations can be written:

$$\sigma = \tanh kh, \quad \omega^2 = gk\sigma; \quad (1.2a)$$

$$c_p = \omega/k, \quad c_g = g[\sigma + kh(1-\sigma^2)]/2\omega. \quad (1.2b)$$

Equations (1.2a) give the linear dispersion relation defining the radian frequency ω, where g is the acceleration due to gravity. Equations (1.2b) define the phase and group velocities respectively. We define the parameter

$$\mu = 2\left(\frac{\pi}{\gamma\sigma}\right)^2 \frac{9 - 10\sigma^2 + 9\sigma^4 - 2\sigma^2[4c_p^2 + 4c_p c_g(1-\sigma^2) + gh(1-\sigma^2)^2]\,(gh - c_g^2)^{-\frac{1}{2}}}{[\sigma - kh(1-\sigma^2)]^2 + (2kh\sigma)^2\,(1-\sigma^2)}, \quad (1.3)$$

which will be used in the following discussion.

A normalized complex wave envelope $\psi(x,t)$ is now considered, which is related to the free surface elevation $\eta(x,t)$ by the expression

$$\eta = a\mathscr{R}[\psi e^{i(kx-\omega t)}]. \quad (1.4)$$

The horizontal co-ordinate x and time t are transformed to dimensionless variables ξ and τ, respectively:

$$\xi = \frac{\gamma}{2\pi} ak^2(x - c_g t), \quad \tau = -\frac{(ak)^2}{|\mu|}\omega t. \quad (1.5a, b)$$

In terms of $\psi(\xi,\tau)$, the long-time evolution of a nonlinear wave train like the one defined in (1.1) for water of uniform depth is governed by the NLS equation

$$i\psi_{,\tau}+\psi_{,\xi\xi}+\mu|\psi|^2\psi=0, \tag{1.6}$$

where μ is given by (1.3). The particular choice of co-ordinates (1.5) leads to the canonical form (1.6) of the NLS, periodic in ξ with period 1. The initial condition in terms of ψ is obtained by equating (1.4) to our initial system (1.1). It follows that

$$\psi(\xi,0)=1+2\beta e^{i\alpha}\cos 2\pi\xi. \tag{1.7}$$

The mathematical statement of the problem is now complete. We seek solutions for the complex wave envelope $\psi(\xi,\tau)$, satisfying (1.6), which are periodic in ξ with period unity, and subject to the initial condition (1.7).

The particular choice of identical side-band amplitudes β and phase shifts α was made in order to simplify the presentation. Consideration of two different phase shifts merely results in the addition of a constant to ξ in (1.5a). For different initial amplitudes of the side-band components, it can easily be shown, by means of the so-called second invariant I_2 (§2.1), that their energy difference must remain constant in time. Thus, the initially different (but small) disturbance amplitudes quickly become nearly identical.

2. Approximate analytical solution

2.1. *General properties*

The NLS equation (1.6), with $\xi\in[0,1]$, subject to periodic boundary conditions, has three primitive time invariants.

$$I_1=\int_0^1|\psi|^2d\xi,\quad I_2=\int_0^1(\psi^*\psi_{,\xi}-\psi\psi^*_{,\xi})\,d\xi,\quad I_3=\int_0^1\left(|\psi|^4-\frac{2}{\mu}|\psi_{,\xi}|^2\right)d\xi. \tag{2.1}$$

The boundary conditions and the particular initial condition (1.7), which is even, ensure that the solution $\psi(\xi,\tau)$ is an even function of ξ, symmetrical about $\xi=\frac{1}{2}$. Thus $I_2=0$ and, since $\psi_{,\xi}$ is continuous, $\psi_{,\xi}(0,\tau)=\psi_{,\xi}(\frac{1}{2},\tau)=0$. The latter can be used as equivalent boundary conditions for our particular problem.

2.2. *Fourier analysis*

Let the NLS equation be rewritten as

$$i\psi_{,\tau}+\psi_{,\xi\xi}=-\mu f(\xi,\tau)\quad(f(\xi,\tau)=|\psi|^2\psi), \tag{2.2}$$

for which we seek an approximate solution of the form

$$\psi^N(\xi,\tau)=\sum_{n=-N}^{N}D_n(\tau)\,e^{2\pi in\xi}. \tag{2.3}$$

Note that ψ^N converges in the mean to the solution as $N\to\infty$. Since no discontinuities are present, the convergence is also uniform. ψ^N satisfies the periodic boundary conditions. Moreover, the initial condition implies that

$$D_0(0)=1,\quad D_{\pm1}(0)=\beta e^{i\alpha},\quad D_{\pm n}(0)=0\quad(n>1). \tag{2.4}$$

Substitution of (2.3) in (2.2) reduces the problem to the solution of a set of $N+1$ first-order ordinary differential equations:

$$\frac{dD_n}{d\tau}+i(2\pi n)^2 D_n - i\mu A_n = 0, \quad D_{-n} = D_n \quad (n = 0, 1, \ldots, N), \tag{2.5}$$

subject to the initial conditions (2.4), where A_n are the coefficients in the Fourier expansion of $f(\xi,\tau) \simeq |\psi^N|^2\psi^N$ (also an even function). Thus

$$D_{\pm n}(\tau) = \left[D_n(0) + i\mu\int_0^\tau A_n(t)\, e^{i(2\pi n)^2 t}\, dt\right] e^{-i(2\pi n)^2\tau}, \tag{2.6}$$

with

$$A_n(t) = \int_0^1 f(\xi,t)\, e^{-2\pi i n\xi}\, d\xi = \sum_{k,l,m=-N}^{N}\sum D_k D_l D_m^*(t)\,\delta_{k+l-m,n} \quad (n = 0, 1, \ldots, N). \tag{2.7}$$

The Kronecker δ in (2.7) has the value 1 if $k+l-m = n$, and is zero otherwise.

2.3. *Analytical solution for a simplified system*

Following an approach similar to that of Bryant (1979, §5), we consider that interactions occur mainly between the three central wave modes D_0 (the carrier wave), D_1 and D_{-1} (the side-band components). We therefore neglect the evolution of other components and restrict ourselves to a system (2.5) with $N = 1$, namely

$$i\frac{dD_0}{d\tau}+\mu[(|D_0|^2+4|D_1|^2)D_0+2D_1^2D_0^*] = 0, \tag{2.8a}$$

$$i\frac{dD_{\pm1}}{d\tau}+\mu[(2|D_0|^2+3|D_1|^2-\tfrac{1}{2}P)D_1+D_0^2D_1^*] = 0, \tag{2.8b}$$

where $P = 8\pi^2/\mu$. The set (2.8) is subject to the initial conditions (2.4) and its primitive time invariants are

$$J_1 = |D_0|^2+2|D_1|^2 = 1+\epsilon \quad (\epsilon = 2\beta^2), \tag{2.9a}$$

$$\begin{aligned} J_3 &= |D_0|^4+6|D_1|^4+8|D_0|^2|D_1|^2-2P|D_1|^2+2(D_0^2D_1^{*2}+D_0^{*2}D_1^2) \\ &= 1+(4-P+2\cos 2\alpha)\epsilon+\tfrac{3}{2}\epsilon^2. \end{aligned} \tag{2.9b}$$

We note that substitution of $\psi^1(\xi,\tau)$ from (2.3) into (2.1), and use of $D_1(\tau) = D_{-1}(\tau)$ lead to $J_1 \equiv I_1$, $J_3 \equiv I_3$ and $I_2 \equiv 0$, which indicate the equivalence between the NLS and (2.8) for the simplified system. Multiplying (2.8b) by D_1^* and subtracting the conjugate of the resulting expression, we arrive at

$$\frac{id|D_1|^2}{d\tau} = -\mu(D_0^2D_1^{*2}-D_0^{*2}D_1^2) = -2\mu i\mathscr{I}(D_0^2D_1^{*2}). \tag{2.10}$$

The real part of $D_0^2D_1^{*2}$ can be obtained from (2.9b) as

$$4\mathscr{R}(D_0^2D_1^{*2}) = J_3-|D_0|^4-6|D_1|^4-8|D_0|^2|D_1|^2+2P|D_1|^2. \tag{2.11}$$

Adding the squares of (2.10) and (2.11) and using (2.9a) leads to the following equation for the side-band disturbance energy $Z = 2|D_1|^2$:

$$\frac{1}{\mu^2}\left(\frac{dZ}{d\tau}\right)^2 = [2Z(J_1-Z)]^2-[J_3-\tfrac{3}{2}Z^2-(J_1-Z)^2-4Z(J_1-Z)+PZ]^2. \tag{2.12}$$

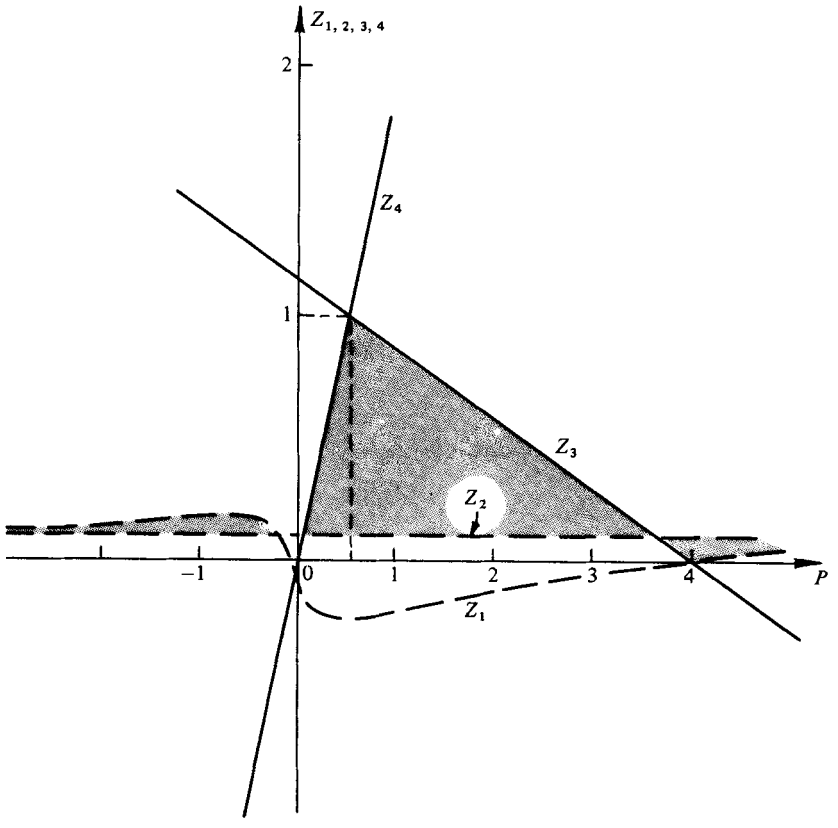

FIGURE 1. The range of variation of Z, for the case $\alpha = 0$.

The right-hand side of (2.12) is a fourth-order polynomial in Z, $Q(Z)$, whose roots are

$$\left.\begin{aligned} Z_{1,4} &= P\{1 \pm [1+2(J_3-J_1^2)/P^2]^{\frac{1}{2}}\}, \\ Z_{2,3} &= \tfrac{1}{7}(4J_1-P)\{1 \pm [1-14(J_3-J_1^2)/(4J_1-P)^2]^{\frac{1}{2}}\}. \end{aligned}\right\} \tag{2.13}$$

Introducing the values of J_1 and J_3 computed from the initial conditions, and expressed in (2.9), the roots (2.13), accurate to order ϵ, become

$$\left.\begin{aligned} Z_1 &= \epsilon[1-4P^{-1}\cos^2\alpha], \\ Z_2 &= \epsilon[1-4(4-P)^{-1}\sin^2\alpha], \\ Z_3 &= \tfrac{2}{7}(4-P)+[\tfrac{1}{7}+4(4-P)^{-1}\sin^2\alpha]\epsilon, \\ Z_4 &= 2P-[1-4P^{-1}\cos^2\alpha]\epsilon. \end{aligned}\right\} \tag{2.14}$$

We note that all four roots are real and that two of them ($Z_{1,2}$ in (2.14)) are always in a neighbourhood of order ϵ about the initial value $Z(0) = \epsilon$. The value of α determines which is the largest between these two roots.

The variation of the roots with P for the case $\alpha = 0$ is illustrated in figure 1. The lines for Z_3 and Z_4 were plotted to $O(1)$, and those corresponding to Z_1 and Z_2 were sketched to $O(\epsilon^2)$. Since $Q(Z)$ must be positive (left-hand side of (2.12)), and Z varies continuously starting from $Z(0) = \epsilon$, the admissible variation range is the shaded area in figure 1. This is illustrated in figure 2 where sketches of $Q(Z)$ at three representative sections $P < 0$, $P > 4$ and $0 < P < 4$ are presented. In the first two cases

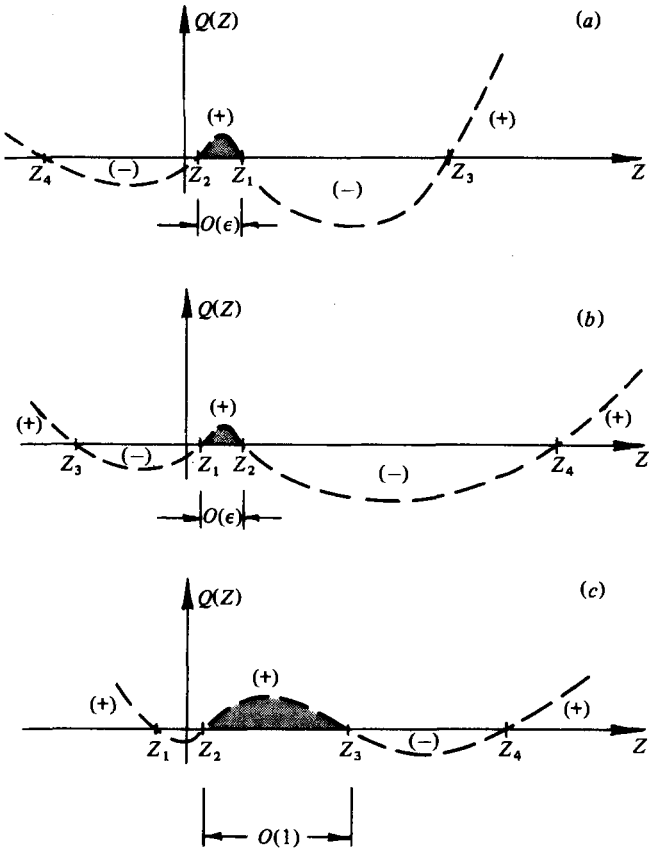

FIGURE 2. Range of definition of Z for: (*a*) $P < 0$, (*b*) $P > 4$ and (*c*) $0 < P < 4$.

(*a*), (*b*), the admissible range of variation of Z is bound to the small interval between Z_1 and Z_2. Thus, the evolution of the disturbance remains of $O(\epsilon)$ and the solution is stable. In the third case (*c*), both Z_1 and Z_2 are located to the left of ϵ while Z_3 and Z_4 are located to the right. The relative locations of Z_3 and Z_4 are determined by the limit $P = \frac{1}{2} + O(\epsilon)$ while the relative locations of Z_1 and Z_2 are determined by the limit $P = 4\cos^2\alpha + O(\epsilon^2)$. For case (*c*), the admissible range of variation of Z becomes $O(1)$, so that the disturbance may grow from its initial value ϵ to $\frac{2}{7}(4-P) + O(\epsilon)$.

In the following, we refer to the cases where the simplified solution is applicable, namely $1 < P < 4$ (see §2.6), and rename the roots $Z_{1,2} = c, d$, $Z_3 = b$, $Z_4 = a$ so $a > b > Z \geqslant c > d$. The evolution of the perturbation energy Z is found by integrating (2.12) in the form:

$$\mu\tau = \int_{\epsilon}^{Z} dy\,[Q(y)]^{-\frac{1}{2}} \quad (c \leqslant Z < b). \tag{2.15}$$

Following Byrd & Friedman (1971, p. 116), we develop the right-hand side of (2.15) and, after some algebraic manipulations, we eventually arrive at

$$\frac{b-Z}{a-Z} = \frac{b-\epsilon}{a-\epsilon}\left[\frac{1-\dfrac{a-b}{a-\epsilon}\left(\dfrac{(\epsilon-c)(\epsilon-d)}{(b-c)(b-d)}\right)^{\frac{1}{2}}\dfrac{\mathrm{sd}}{\mathrm{cn}}}{1+\dfrac{(a-b)(a-d)(\epsilon-c)}{(a-\epsilon)(b-d)(a-c)}\,\mathrm{sd}^2}\right]\mathrm{cd}^2, \tag{2.16}$$

where $\mathrm{sd} = \mathrm{sn}/\mathrm{dn}$, $\mathrm{cd} = \mathrm{cn}/\mathrm{dn}$ represent Jacobian elliptic functions of argument $-\frac{1}{4}[7(a-c)(b-d)]^{\frac{1}{2}}\mu\tau$ and modulus κ, with

$$\kappa^2 = \frac{(b-c)(a-d)}{(a-c)(b-d)}.$$

We note that the terms $\epsilon - c$ and $\epsilon - d$ in (2.16) are $O(\epsilon)$, so the square brackets have essentially the value 1. Hence (2.16) can be written

$$\frac{b-Z}{a-Z} = \frac{b}{c}\mathrm{cd}^2(-\tfrac{1}{4}(7ab)^{\frac{1}{2}}\mu\tau, \kappa) + O(\epsilon) \quad \text{or} \quad Z = \frac{ab(1-\mathrm{cd}^2)}{a - b\,\mathrm{cd}^2} + O(\epsilon). \tag{2.17}$$

More explicitly, the energy of the pair of side-band disturbance components evolves in time according to

$$Z = \frac{2P(4-P)\,[1-\mathrm{cd}^2(-\frac{1}{2}(P(4-P))^{\frac{1}{2}}\mu\tau, \kappa)]}{7P-(4-P)\,\mathrm{cd}^2(-\frac{1}{2}(P(4-P))^{\frac{1}{2}}\mu\tau, \kappa)} + O(\epsilon). \tag{2.18}$$

Expression (2.18) is periodic, with the period $\bar{\tau}$ governed by the behaviour of the cd^2 function.†

Since

$$\kappa^2 = 1 - \frac{8\epsilon(2P-1)\,|4\cos^2\alpha - P|}{P^2(4-P)^2} + O(\epsilon^2) \leqslant 1$$

is nearly unity, we may write (see Byrd & Friedman 1971, equation 112.01)

$$\mu\bar{\tau} = \frac{2}{(P(4-P))^{\frac{1}{2}}} \ln\left[\frac{P^2(4-P)^2}{(2P-1)\,|4\cos^2\alpha - P|\,\beta^2}\right] \quad (\kappa \to 1). \tag{2.19}$$

If $4\cos^2\alpha = P$, then Z_1 and Z_2 become $O(\epsilon^2)$ and (2.19) is modified accordingly to read

$$\mu\bar{\tau} = \frac{2}{(P(4-P))^{\frac{1}{2}}} \ln\left[\frac{P^2(4-P)^2}{(2P-1)\,\beta^4}\right] \quad (\kappa \to 1). \tag{2.20}$$

2.4. *The onset of growth*

We now consider the asymptotic behaviour of Z for $\tau \to 0$, through the Taylor expansion

$$Z = Z(0) + \left.\frac{dZ}{d\tau}\right|_{\tau=0} \tau + O(\tau^2). \tag{2.21}$$

Computing the exact expressions for the derivatives from (2.10) and substituting $Z(0) = \epsilon$, we obtain

$$Z = \epsilon(1 + 2\mu\tau\sin 2\alpha) + O(\tau^2) \quad (\tau \to 0). \tag{2.22}$$

From this expression, we see that, as long as τ is small, Z remains of $O(\epsilon)$. However, as time elapses and Z becomes $\gg O(\epsilon)$ but still $Z \ll \frac{2}{7}(4-P)$, we can refer to (2.12), neglecting terms of $O(\epsilon)$ when compared with Z, and terms in Z when compared to either P or $4-P$. For that range of τ, (2.12) reduces to

$$\frac{dZ}{d\tau} = \pm\mu(P(4-P))^{\frac{1}{2}} Z. \tag{2.23}$$

† Note that, if $\kappa \equiv 1$ (no disturbance), then $\mathrm{cd} \equiv 1$ and $Z \equiv 0$, so $|\psi^1| \equiv 1$. This bears some resemblance to the elementary example $du/dt = -(1-u^2)^{\frac{1}{2}}$ with $u(0) = 1$. The trivial solution $u = 1$ is unstable to disturbances in the initial condition, giving rise to the oscillatory solution $u = \cos t$.

The solution of (2.23) that matches expression (2.22) for small values of τ is

$$Z = \tfrac{1}{2}\epsilon\left[1+\frac{2\sin 2\alpha}{(P(4-P))^{\frac{1}{2}}}\right]\exp\{(P(4-P))^{\frac{1}{2}}\mu\tau\} + \tfrac{1}{2}\epsilon\left[1-\frac{2\sin 2\alpha}{(P(4-P))^{\frac{1}{2}}}\right]\exp\{-(P(4-P))^{\frac{1}{2}}\mu\tau\}. \quad (2.24)$$

The latter expressions indicate an exponential growth, whose fastest rate, in terms of $\mu\tau$, occurs for $P = 2$, in accordance with Benjamin & Feir (1967).

2.5. *The evolution of the wave envelope* $|\psi^1(\xi,\tau)|$

Taking the modulus of $\psi^1(\xi,\tau) = D_0 + 2D_1\cos 2\pi\xi$, we obtain

$$|\psi^1|^2 = J_1 - Z + 2Z\cos^2 2\pi\xi + 2(D_0 D_1^* + D_0^* D_1)\cos 2\pi\xi. \quad (2.25)$$

Substituting in (2.25) the identity

$$D_0 D_1^* + D_0^* D_1 \equiv S[(D_0^2 D_1^{*2} + D_0^{*2} D_1^2) + Z(J_1 - Z)]^{\frac{1}{2}}, \quad (2.26)$$

where S is the sign of $\cos\alpha$,† and noting that the expression in square brackets in (2.26) can be obtained as a function of Z from the J_3 invariant (2.9*b*), one arrives at

$$|\psi^1|^2 = \{-2(J_3 - J_1^2) + 2(4J_1 - P)Z - 7Z^2 + [S(2(J_3 - J_1^2) + 2PZ - Z^2)^{\frac{1}{2}} + 4Z\cos 2\pi\xi]^2\}/8Z. \quad (2.27)$$

Equation (2.27) can be rewritten in the form

$$|\psi^1|^2 = \tfrac{1}{4}(4-P) - \tfrac{7}{8}Z + \tfrac{1}{8}(S(2P-Z)^{\frac{1}{2}} + 4Z^{\frac{1}{2}}\cos 2\pi\xi)^2 + O(\epsilon). \quad (2.28)$$

The explicit evolution of $|\psi^1|^2$ is found by substituting in (2.28) the expression (2.18) for Z, which eventually leads to

$$|\psi^1|^2 = \frac{(4-P)(2P-1)\,\mathrm{cd}^2 + P\{S(2P-1)^{\frac{1}{2}} + 2[(4-P)(1-\mathrm{cd}^2)]^{\frac{1}{2}}\cos 2\pi\xi\}^2}{7P-(4-P)\,\mathrm{cd}^2}. \quad (2.29)$$

Equating to zero the derivative of (2.29) with respect to ξ, it can be seen that maxima and minima occur only at $\xi = 0$ and $\xi = \frac{1}{2}$ (of course, the solution is symmetric about $\xi = \frac{1}{2}$). The derivative of (2.29) also vanishes at

$$\xi_{\mathrm{m}} = \frac{1}{2\pi}\arccos\left[-\frac{S}{2}\left(\frac{2P-1}{(4-P)(1-\mathrm{cd}^2)}\right)^{\frac{1}{2}}\right], \quad (2.30)$$

if the argument of the arccosine function falls within the admissible range $(-1, 1)$. Thus, whenever $\mathrm{cd}^2 < 1 - \frac{1}{4}(2P-1)(4-P)^{-1}$ (which can only occur for $P < \frac{17}{6} \simeq 2{\cdot}83$), $|\psi^1|$ has a minimum at ξ_m. On the other hand, for τ close to zero, or for all τ when $P > 2{\cdot}83$, expression (2.30) is insignificant and $|\psi^1|$ is monotonic in $0 \leqslant \xi \leqslant \frac{1}{2}$.

2.6. *The range of applicability of the solution*

Among the assumptions made in § 1, we considered the γ parameter to be $O(1)$, so $\Delta k/k$ is of the order of the (small) slope ak. Referring to (2.3) for ψ^N, pairs of terms of index n and $-n$ are regarded as symmetric side-band components with $\Delta k/k$ replaced by

$$n\,\Delta k/k = n\gamma ak \quad (n = 1, 2, \ldots, N). \quad (2.31)$$

† The marginal cases where $\cos\alpha = 0$ are excluded from this analysis.

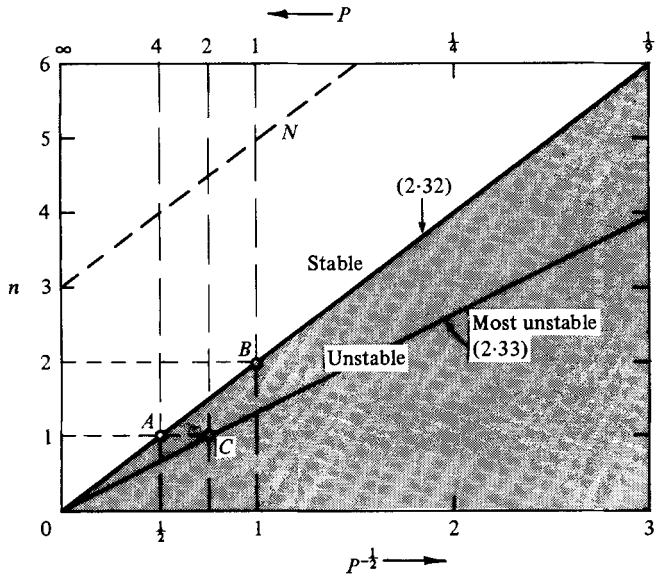

FIGURE 3. Stability and instability regions for the side-band pairs of components.

Here, $n\gamma$ replaces γ so, from (1.3), μ/n^2 should replace μ. Recalling that $P = 8\pi^2/\mu$, and the stability limit $P > 4$ (see figure 1), it follows that

$$n^2P > 4 \quad \text{(i.e.} \quad n > 2P^{-\frac{1}{2}}) \tag{2.32}$$

implies stability of the nth pair of side-band components. In an analogous way

$$n^2P = 2 \quad \text{(i.e.} \quad n = (2/P)^{\frac{1}{2}}) \tag{2.33}$$

indicates the most unstable behaviour of pair n (see §2.4). These limits are illustrated in figure 3, where n is plotted versus both $P^{-\frac{1}{2}}$ and P.

From this figure, it can be seen that, in the range $P > 4$ ($P^{-\frac{1}{2}} < \frac{1}{2}$), even the first pair of side-band disturbance components ($n = 1$) is stable. At $P = 4$ the $n = 1$ pair enters the unstable interaction region (point A). In the range $4 > P > 1$ only this $n = 1$ pair is unstable, the most unstable case occurring at $P = 2$ (point C). At $P = 1$ the second pair of side-band components $n = 2$ enters the instability region (point B). Thus, the proposed approximate solution, which assumes only one pair of unstable disturbance components, is invalid for $P < 1$. The value $P = 1$ is the limit between the 'simple' and 'complex' evolutions referred to by Yuen & Ferguson (1978). For a given value of P (or μ), the number of modes actively participating in the energy exchange with the carrier can be easily found from figure 3.

A sufficient number N of modes to be considered in the expression (2.3) for ψ^N in the Fourier analysis of §2.2, and in its actual computation (as described in §3.1) for a particular value of P, is obtained when taking, say, 3 pairs of components within the stability region, as indicated by the N-line of figure 3.

3. Comparison between the analytical and numerical solutions

3.1. *The reference solution*

In order to appraise the validity of the behaviour predicted by the approximate analytical solution just described, a presumably 'exact' reference solution, which is free of limiting assumptions, is necessary. The reference solution for the problem stated in § 1.2 is obtained by means of numerical schemes. Two independent alternative numerical approaches were employed for that purpose, namely a finite-difference approximation scheme and the evaluation of the Fourier solution of § 2.2 using a sufficient number N of terms.

In the first approach, $J-1$ equal segments $\Delta\xi$ span the interval $0 \leqslant \xi \leqslant \frac{1}{2}$ while equal intervals $\Delta\tau$ span the time co-ordinate. The finite-difference approximation operates on discretized values $\psi_j^n = \psi(\xi_j, \tau_n)$, where $\xi_j = (j-1)\,\Delta\xi$ and $\tau_n = n\,\Delta\tau$. A standard iterative Crank–Nicholson scheme is written

$$i\frac{\psi_j^{n+1}-\psi_j^n}{\Delta\tau}+\frac{1}{2}\left(\frac{\psi_{j-1}^{n+1}-2\psi_j^{n+1}+\psi_{j+1}^{n+1}}{\Delta\xi^2}+\frac{\psi_{j-1}^{n}-2\psi_j^{n}+\psi_{j+1}^{n}}{\Delta\xi^2}\right)$$
$$+\tfrac{1}{2}\mu\left|\psi_j^{n+\frac{1}{2}}\right|^2(\psi_j^{n+1}+\psi_j^n)=0 \quad (j=1,2,\ldots,J;\ n=0,1,\ldots), \tag{3.1}$$

subject to the initial condition (1.7) and to boundary conditions $\psi_0^n = \psi_2^n$, $\psi_{J+1}^n = \psi_{J-1}^n$. The scheme conserves numerically the first invariant when integrating over ξ by means of the trapezoidal rule, irrespective of the approximation used for $|\psi_j^{n+\frac{1}{2}}|^2$. It gives rise to a tridiagonal system of algebraic equations solved by means of the double-sweep algorithm. The matrix coefficients include $|\psi_j^{n+\frac{1}{2}}|^2$, for which the approximations $|\psi_j^n||\psi_j^{n+1}|$ and $\frac{1}{2}(|\psi_j^n|^2+|\psi_j^{n+1}|^2)$ were tried, yielding almost identical results. The accuracy of the solution was appraised by comparing computed values of I_3^n with the invariant value I_3^0 at time 0. The scheme proved to be stable, and sufficient accuracy was obtained for $J = 24$, $\lambda = \Delta\tau/\Delta\xi^2 = -1$ (negative λ implies advance in physical time; (1.5*b*)) and 3 iterations per time step.

In the second approach, we rewrite (2.6) in the form

$$D_{\pm n}(\tau+\Delta\tau)=\left[D_n(\tau)+i\mu e^{-i(2\pi n)^2\tau}\int_\tau^{\tau+\Delta\tau}e^{i(2\pi n)^2 t}A_n(t)\,dt\right]e^{-i(2\pi n)^2\Delta\tau}$$
$$(n=0,1,\ldots,N), \tag{3.2}$$

and approximate the integral (for sufficiently small $\Delta\tau$) by means of

$$\tfrac{1}{2}[A_n(\tau)+A_n(\tau+\Delta\tau)]\int_\tau^{\tau+\Delta\tau}e^{i(2\pi n)^2 t}\,dt. \tag{3.3}$$

This leads to the expressions

$$\left.\begin{aligned} D_0(\tau+\Delta\tau) &= D_0(\tau)+\tfrac{1}{2}i\mu(A_0(\tau+\Delta\tau)+A_0(\tau)) \quad (n=0),\\ D_{\pm n}(\tau+\Delta\tau) &= fD_n(\tau)+(1-f)\,(A_n(\tau+\Delta\tau)+A_0(\tau))/Pn^2 \quad (n=1,2,\ldots,N),\end{aligned}\right\} \tag{3.4}$$

where $f = e^{-i(2\pi n)^2\Delta\tau}$. The latter expressions, coupled with (2.7), are applied iteratively within a time step. The accuracy of the evaluated expression (2.3) is appraised by comparing computed values of

$$J_1^N(\tau)=|D_0|^2+2\sum_{n=1}^{N}|D_n|^2, \quad J_3^N(\tau)=A_0D_0^*+2\sum_{n=1}^{N}(A_n-Pn^2D_n)\,D_n^* \tag{3.5}$$

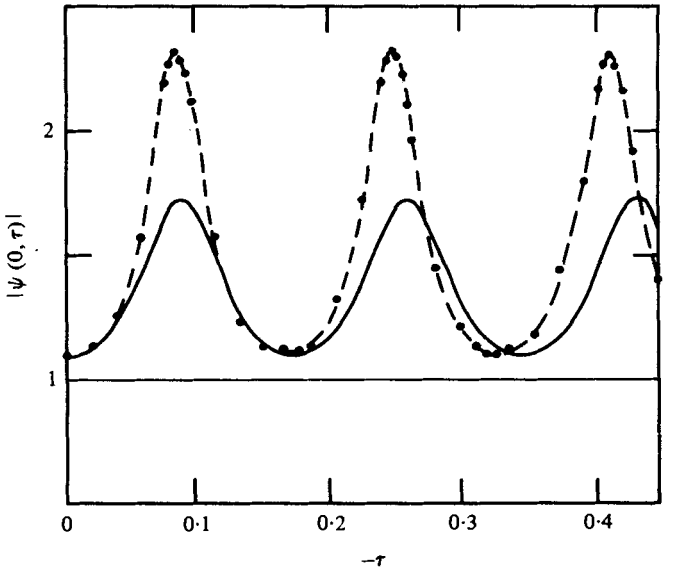

FIGURE 4. The evolution of $|\psi|$ at $\xi = 0$ for $\alpha = 0$, $\beta = 0{\cdot}05$ and $P = 2$.

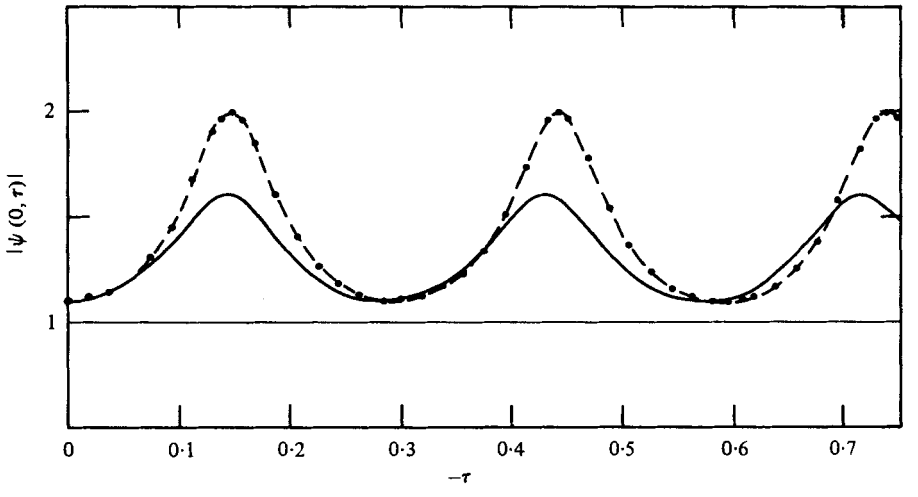

FIGURE 5. The evolution of $|\psi|$ at $\xi = 0$ for $\alpha = 0$, $\beta = 0{\cdot}05$ and $P = 3$.

with the corresponding invariant values at time 0, as given by (2.9). The procedure was, in some aspects, inspired by the work of Gajewsky (1978). Results from sensitivity runs indicate that sufficient accuracy is obtained for $N = 5$, $\Delta\tau = -10^{-3}$, and 5 iterations per time step.

The accuracy of the reference solution is shown by the fact that, with the exception of slight differences at the peaks, both unrelated numerical approaches yield almost identical results.

3.2. *The stability range*

Several runs of the numerical schemes were performed in order to verify the stability range predicted by the approximate analytical solution. For instance, it was verified that $|\psi(\xi,\tau)|$ remains of the order of the initial disturbance for $P = -1$ and $P = 4$.

	α \ P	1·0	1·1	2·0	3·0
$\beta = 0$	$0, \pi$	—	—	1·90 (1·89)	—
$\beta = 0{\cdot}005$	$0, \pi$	—	—	0·29 (0·29)	—
	$\frac{3}{4}\pi$	—	—	0·34 [0·58]	—
		0·08	0·09	0·17	0·30
$\beta = 0{\cdot}05$	$0, \pi$	(0·10)	(0·11)	(0·18)	(0·29)
	$\frac{3}{4}\pi$	—	—	0·29 [0·34]	0·29 (0·29)
	$\frac{1}{2}\pi$	—	—	0·17 (0·18)	—

TABLE 1. The modulation–demodulation cycle period $\bar{\tau}$ for various values of P, α and β

Also, 'complex'-type evolutions were obtained for $P = 0{\cdot}5$ and $P = 0{\cdot}2$ which, according to figure 3, involve 2 and 4 unstable pairs of side-band components, respectively. Sections 3.3, 3.4 refer to numerical runs in the range of applicability of the simplified analytical solution, i.e. $1 < P < 4$.

3.3. *Comparison of envelope profiles* $|\psi(\tau)|$ *at* $\xi = 0$

We have chosen to present some particular representative sections of the wave envelope, namely, $|\psi(0,\tau)|$ for $\alpha = 0$, $\beta = 0{\cdot}05$ and $P = 2$ and 3 (figures 4 and 5 respectively). The values of τ are negative, so they correspond to positive physical time (see (1.5*b*)). Full lines in these figures represent the analytical profiles $|\psi^1(0,\tau)|$, computed from expressions (2.16) and (2.27), while dotted lines are the results from the numerical solutions.

In figures 4 and 5 it is seen that the peak values of $|\psi|$ from the numerical solutions are 2·4 and 2·0 for $P = 2$ and $P = 3$, respectively. On the other hand, the analytical solution allows for a maximum value $|\psi^1| = 3^{\frac{1}{2}}$, corresponding to an equal energy distribution between the carrier and the single pair of side-band components. However, much better agreement is obtained when comparing modulation–demodulation cycle periods $\bar{\tau}$. The reference periods are measured between successive peaks in $|\psi(0,\tau)|$ from the numerical solutions.

More results are summarized in table 1, where the values enclosed in parentheses were calculated from (2.19) while those in square brackets are from (2.20). It can be seen, from figures 4 and 5 and table 1, that the values predicted by (2.19) are in pretty good agreement with results from the numerical solutions, while those from (2.20) are rather large. The $\beta = 0$ case corresponds to an initial condition where only numerical background noise (of the order $\beta \sim 10^{-16}$) was present.

3.4. *Comparison of envelope profiles* $|\psi(\xi)|$ *at selected values of* τ

We have chosen to present some sections of the envelope at fixed values of τ corresponding to the most modulated states. In terms of the simplified analytical solution, the most modulated situation occurs when the disturbance energy Z is largest

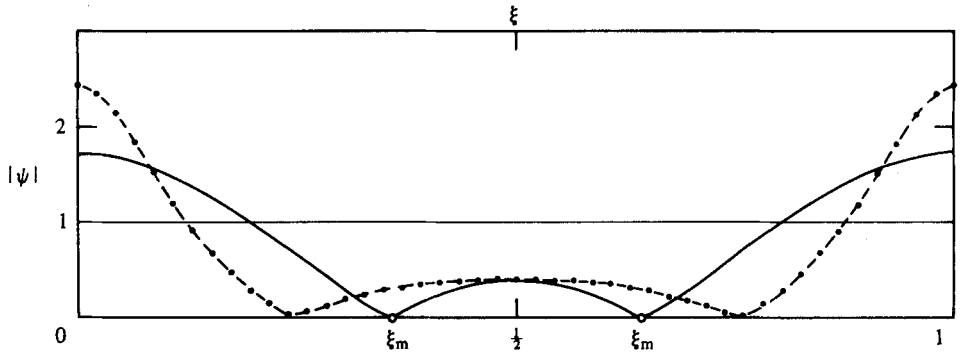

FIGURE 6. The shape of $|\psi|$ versus ξ at the most modulated situation, for $P = 2$.

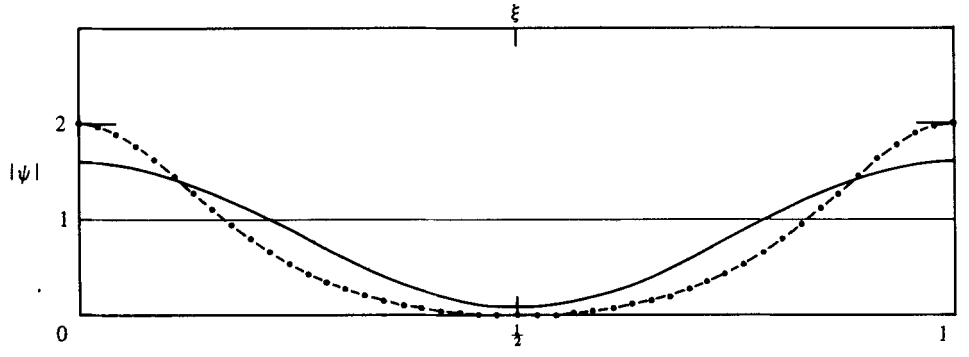

FIGURE 7. The shape of $|\psi|$ versus ξ at the most modulated situation, for $P = 3$.

($Z = b \simeq \frac{2}{7}(4-P)$ in (2.27)) i.e. when cd = 0. Figure 6 corresponds to $P = 2$, $\beta = 0{\cdot}05$ and $\alpha = 0$. The values ξ_m predicted by expression (2.30) with cd = 0 are indicated. Dotted lines represent the numerical solutions, while full lines are plots of the simplified analytical solution $|\psi^1|$. A case in which $|\psi|$ is monotonic in $0 \leqslant \xi \leqslant \frac{1}{2}$ for all τ (and, in particular, at the most modulated states) is illustrated in figure 7 for $P = 3$, $\beta = 0{\cdot}05$ and $\alpha = 0$.

Inspection of figures 4–7 and table 1 shows that, although different in detail, the general features of the reference numerical solution behave essentially as predicted by the expressions of the approximate analytical solution. In particular, the presence or absence of a minimum in $0 \leqslant \xi \leqslant \frac{1}{2}$ according to the value of P (see §2.5) was correctly predicted. An extremely important feature concerns the uniqueness of the $|\psi|$ versus ξ shape at the most modulated situations. The analytical envelope shape $|\psi^1|$ of (2.29) indicates a weak dependence on the initial-condition parameters α and β. The dependence however exists through the $O(\epsilon)$ terms and modulus of cd in that expression, and governs the onset of the evolution. Nevertheless, at the most modulated situations (cd = 0 in (2.29)), $|\psi^1(\xi)|$ is only dependent on P.†

This important property was verified for $P = 2$ and $P = 3$ by running the numerical solutions with different values of α and β and superimposing $|\psi|$ versus ξ profiles corresponding to the most modulated situations. In particular, the dotted lines of

† The influence of α on $|\psi^1|$ through S, (2.29), is of minor importance. Its effect is at most a shift of $\frac{1}{2}$ in ξ.

figures 6 and 7, which were plotted from runs with $\beta = 0{\cdot}05$ and $\alpha = 0$, are identical with the profiles obtained from runs with $\beta = 0{\cdot}005$ and/or $\alpha = -\frac{1}{4}\pi$.

4. Physical considerations

4.1. *The power of the simplified analytical solution*

From the comparison of results with reference numerical solutions it becomes clear that, although the simplified analytical solution yields poor quantitative results for the envelope amplitude, it is an extremely powerful tool for predicting qualitative features of the solution and general trends. In particular, correct predictions for the general recurrence phenomenon are recognized, as well as the instability ranges where it occurs.

Having gained confidence in the power of the approximate solution, we take advantage of it to draw a few implications of practical significance.

4.2. *The influence of the initial disturbance on the long-time evolution*

Three parameters characterize the initially disturbed system: α, β and γ, see (1.1). γ enters the solution explicitly through the μ coefficient defined in (1.3), which multiplies the nonlinear term in the NLS equation (1.6). In the analytical solution, $P = 8\pi^2/\mu$ is used to represent this parameter. γ also enters the solution implicitly through the dimensionless variable ξ, (1.5*a*). The physical time variation of the solution appears, on the other hand, in terms of $\mu\tau$, which does not depend on γ, (1.5*b*). However, γ is involved in the physical time variation through ξ.

The influence of γ through P and ξ on the solution (2.29) is by far the strongest among the three parameters. Irrespective of the exact amplitude β and phase α of the initial disturbance, it determines its range of stability (§2.6) and the shape of the envelope at the most modulated states. Also, the value of γ for which $P = 2$ determines the fastest rate of growth of the disturbance (§2.4). Concerning the latter, it seems plausible that disturbances with that particular value of γ will be selected by nature to dominate the long-time cyclic evolution of an originally uniform wave train (see Longuet-Higgins 1980).

The most important feature of the solution (2.29) is its cyclic nature, oscillating periodically between an almost uniform wave-train state (cd $\sim$ 1) and a most modulated situation (cd = 0). From expressions (2.19) and (2.20) it is seen that the period of the modulation–demodulation cycle is governed by the initial disturbance amplitude β and, to a lesser extent, by α and γ. In terms of dimensional time, this period T_3 is given by

$$T_3 = \mu\bar{\tau}\omega^{-1}(ak)^{-2}, \tag{4.1}$$

where $\mu\bar{\tau}$ is given by (2.19) or, in the case where $4\cos^2\alpha = P$, by (2.20). We note that our approach is invalid in the vicinity of $kh = 1{\cdot}363$ where $\mu = 0$. In that event, the NLS equation (1.6) is not sufficient to model the evolution of the system and higher-order terms are required (see Johnson 1977). Restricting ourselves to $\mu > 0$, it seems, from (2.22) and the second term of (2.24) that, in terms of physical time $\mu\tau$, the fastest growth at the onset of the evolution is obtained (besides $P = 2$) for $\sin 2\alpha = -1$. One

could thus speculate about the priority of disturbances having $\alpha = -\frac{1}{4}\pi, \frac{3}{4}\pi$, at least for the very early stage of the evolution.†

If it proves to be correct that nature selects the fastest growing mode ($P = 2$, $\alpha = \frac{1}{4}\pi, \frac{3}{4}\pi$) to dominate the long-time evolution, then the modulation–demodulation period can be estimated approximately from (4.1) and (2.20), which yield

$$T_3 = \omega^{-1}(ak)^{-2}\ln(16/3\beta^4) = \omega^{-1}(ak)^{-2}(1{\cdot}674 - 4\ln\beta). \tag{4.2a}$$

For other values of α (but still with $P = 2$), T_3 is sufficiently well represented by the expression

$$T_3 = \omega^{-1}(ak)^{-2}\ln(8/3\beta^2) = \omega^{-1}(ak)^{-2}(0{\cdot}981 - 2\ln\beta). \tag{4.2b}$$

This expression is exact for $\alpha = 0$ and $\alpha = \pi$. Expressions (4.2) illustrate the most relevant influence of β on the solution. To our knowledge no such expressions for predicting the modulation–demodulation period have been published previously.

4.3. *Characteristic time and length scales*

The unstable evolution of nonlinear wave trains displays three different time scales, namely:

$$\left.\begin{aligned} &\text{the wave period} \quad T_1 = 2\pi/\omega, \\ &\text{the modulation period} \quad T_2 = 2\pi/\Delta k\, c_g = 2\pi/\gamma ak^2 c_g, \end{aligned}\right\} \tag{4.3}$$

and the modulation–demodulation period T_3. As a first guess, the choice $\beta = O(ak)$ in (4.1), (4.2) for T_3 seems plausible, and leads to $T_3 \simeq T_2/ak$. The modulation period T_2 is implicit in the solution (2.29) through the ξ variable (recall the definition (1.5a) of ξ). Again, the most relevant value of γ to be considered for T_2 is perhaps the one corresponding to $P = 2$, i.e. $\mu = (2\pi)^2$ in (1.3). In particular, for deep water $\sigma = 1$, $\omega^2 = kg$ and $c_g = \omega/2k$ (see (1.2)). Thus (1.3) becomes

$$\mu = 8\pi^2/P = (4\pi/\gamma)^2,$$

which, for $P = 2$, indicates $\gamma = 2$. In this event, (4.3) reduces to

$$T_2 = 2\pi/\omega ak = T_1/ak \quad \text{(deep water)}. \tag{4.4}$$

In order to visualize the three characteristic time scales, a sketch of the water surface variation in time $\eta(t)$, at a fixed location x, for the case $P = 2$, $\alpha = \frac{3}{4}\pi$, $\beta = 0{\cdot}1$, is illustrated in figure 8. As an example, let us consider a 60 m long, 1·5 m high wave in deep water. Hence $T_1 \simeq 6{\cdot}2$ s, $T_2 \simeq 1\frac{1}{3}$ min and $T_3 \simeq 15$ min ((4.2b) with $\beta = 0{\cdot}1$) or $T_3 \simeq 29$ min ((4.2a) with $\beta = 0{\cdot}1$). In an analogous way, the shapes of the water surface $\eta(x)$ at instants t corresponding to an intermediate state and to the most modulated state are sketched in figure 9(a) and (b), respectively. Note that the wave groups appear to contain half the number of individual waves in space as they do in time.

Two length scales are characteristic of the problem, namely:

$$\begin{aligned} &\text{the wavelength} \quad L_1 = 2\pi/k, \\ &\text{the group length} \quad L_2 = L_1/\gamma ak. \end{aligned}$$

† From (2.22) we note that, at the very early stage, the growth is linear and independent of P. Whenever $\sin 2\alpha = 0$, the growth is initially parabolic in $\mu\tau$. Immediately after, the growth becomes exponential, as indicated by (2.24). This behaviour bears some resemblance with the well-known combined Phillips–Miles mechanism in the context of wave generation by wind.

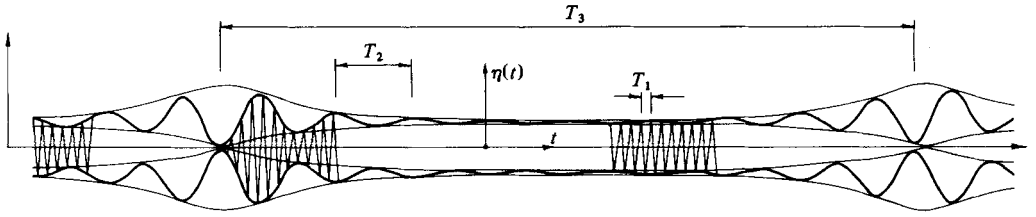

FIGURE 8. Sketch of the surface elevation η at a fixed point, as a function of time t.

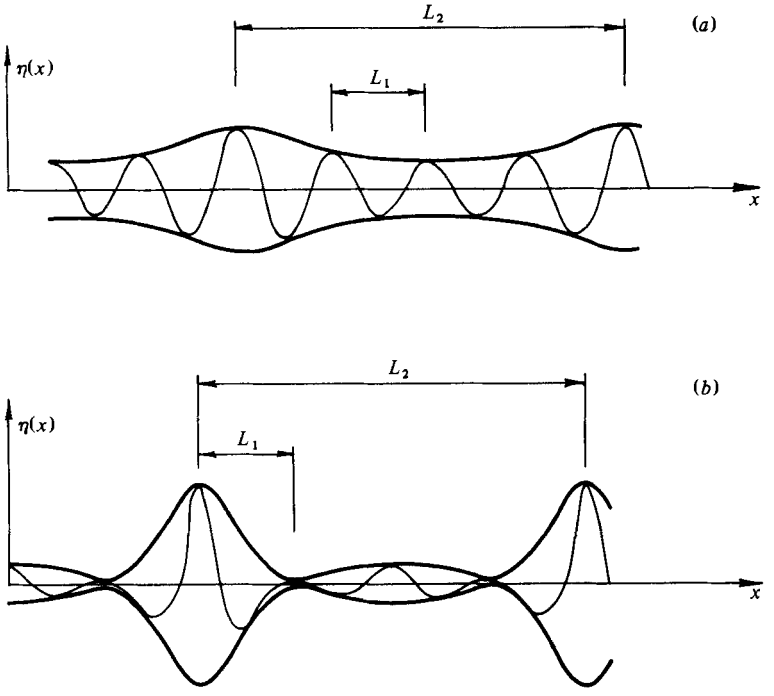

FIGURE 9. Sketch of the surface elevation η as a function of the horizontal distance x, for: (*a*) an intermediate state, and (*b*) the most modulated state.

For the previous deep-water example, $L_1 = 60$ m and $L_2 \simeq 382$ m. Inspection of figure 8 shows that, for the particular case sketched, the ratio between the duration of a state where the wave train is almost uniform to that where it is strongly modulated is about 2 to 1. This ratio becomes smaller for other values of α. In figures 8 and 9 one can see how an initially uniform wave-train state evolves to a most modulated situation resembling envelope solitons containing waves that are much higher and much smaller than the original ones.

Note that one could reproduce the entire analysis of this paper by interchanging space and time, if the problem was stated in terms of a periodic disturbance in time at a fixed point x. In that case, our original NLS equation (1.6) should be replaced by a simplified version of Djordjević & Redekopp's (1978) equation (2.14).

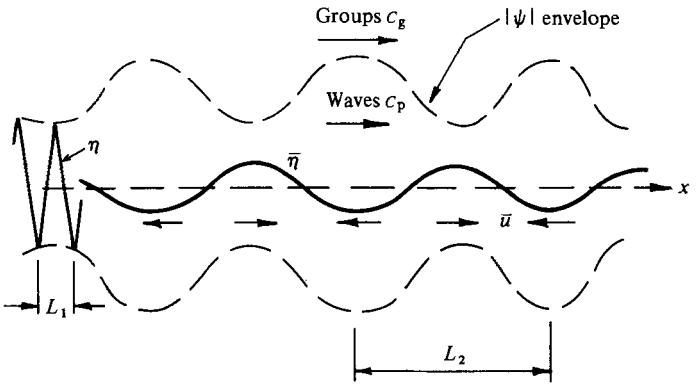

FIGURE 10. Schematic view of the mean free surface $\bar{\eta}$ and direction of the mean current $\bar{u}$.

4.4. *Mean surface level and mean current*

The modulation–demodulation process gives rise to changes in the mean free-surface level $\bar{\eta}$, relative to that of the uniform wave train. Following Davey & Stewartson (1974, equation (2.23)), and using our notation, this is given by

$$k\bar{\eta}(x,t) = -\frac{(ak)^2[(1-\sigma^2)+\sigma/2kh]}{2\sigma(1-c_g^2/gh)}(|\psi^1|^2-1), \tag{4.5}$$

where most symbols are defined in §1.2 and $|\psi^1|^2$ is given in §2.5. In a similar way, the mean current $\bar{u}$ for zero mass flux, can be written as

$$\bar{u}(x,t)/c_g = -(ak)^2\frac{[(1-\sigma^2)+2c_p/c_g]}{4\sigma kh(1-c_g^2/gh)}(|\psi^1|^2-1). \tag{4.6}$$

Expressions (4.5) and (4.6) correspond in principle to a long wave whose length is the length of the group L_2 and whose speed of propagation is the group velocity c_g. This is illustrated schematically in figure 10, where the wave envelope is represented by dashed lines, the mean free surface level by a full line, and the direction of the mean current by arrows.

The minus sign in (4.5) and (4.6) indicates a relative depression in the mean free-surface level beneath the higher waves, coupled with a mean flow in the direction opposite to that of the wave propagation. The highest value that $|\psi^1|^2-1$ can attain is 2. However, values as high as 5 are to be expected from the reference solution.

For deep water, (4.5) and (4.6) vanish, and expressions for $\bar{\eta}$ and $\bar{u}$ would have to include terms of $O((ak)^3)$. Referring to Dysthe (1980), when his equations (4.2) and (4.3) are solved, for the case of very deep water,† the following expressions are obtained, and replace (4.5) and (4.6), respectively:

$$k\bar{\eta}(x,t) = -\tfrac{1}{4}\gamma(ak)^3(|\psi^1|^2-1) \quad \text{(very deep water)}, \tag{4.7}$$

$$\bar{u}(x,t)/c_g = -2\gamma(ak)^3[(D_0D_1^* + D_0^*D_1)e^{2\pi\zeta}\cos 2\pi\xi + 2|D_1|^2 e^{4\pi\zeta}\cos 4\pi\xi]. \tag{4.8}$$

Here, ζ represents the dimensionless vertical co-ordinate‡

$$\zeta = \frac{\gamma}{2\pi}(ak)\,ky,$$

and all other symbols were defined in §§1.2 and 2.3.

† Meaning deep even with respect to the length of the group, i.e. $\Delta kh \gg 1$ or $\gamma ak^2h \gg 1$.

‡ $y = 0$ at the reference mean free surface and is positive upwards.

In the vicinity of the free water surface, or 'upper layer', for which $\zeta \to 0$, (4.8) reduces to

$$\bar{u}(x,t)/c_g = -\gamma(ak)^3(|\psi^1|^2 - 1). \tag{4.9}$$

Expression (4.7) is in agreement with Longuet-Higgins & Stewart (1964).

4.5. *Conclusions*

An analytical solution is proposed for the long-time evolution of a simplified system, where interactions are allowed to take place between a carrier wave and only one pair of side-band components.

It is shown that a 'simple' unstable evolution occurs only in the range $1 < P < 4$. The evolution is periodic in time and the period is governed by the natural logarithm of the initial side-band disturbance energy. This energy oscillates between $O(\epsilon)$ and a maximum value of about $\frac{2}{7}(4-P)$. It is also suggested that the fastest rate of disturbance energy growth occurs for $P = 2$ and $\sin 2\alpha = -1$.

Although a system allowing for more interacting components must be considered, we feel that the approximate analytical solution yields a reliable qualitative indication of the general trends and behaviour of the recurrence phenomenon, especially during the onset of the process, where little energy has dispersed out of or entered the simplified system. Our confidence in the capabilities of the analytical solution stems from its favourable comparison with reference results from two independent numerical approaches to the solution of the NLS equation.

The analytical solution is helpful in visualizing the evolution of the water surface level in space and time and in deriving the relevant characteristic scales. Also, it leads to approximate expressions for the mean free-surface variation and mean current.

REFERENCES

Benjamin, T. B. & Feir, J. E. 1967 The disintegration of wave trains on deep water. Part 1. Theory. *J. Fluid Mech.* **27**, 417–430.

Bryant, P. J. 1979 Nonlinear wave groups in deep water. *Stud. Appl. Math.* **61**, 1–30.

Byrd, P. F. & Friedman, M. D. 1971 *Handbook of Elliptic Integrals for Engineers and Scientists.* Springer.

Davey, A. & Stewartson, K. 1974 On three-dimensional packets of surface waves. *Proc. R. Soc. Lond.* A **338**, 101–110.

Djordjević, V. D. & Redekopp, L. G. 1978 On the development of packets of surface gravity waves moving over an uneven bottom. *Z. angew. Math. Phys.* **29**, 950–962.

Dysthe, K. B. 1980 Note on a modification to the nonlinear Schrödinger equation for application to deep water waves. *Proc. R. Soc. Lond.* A **369**, 105–114.

Gajewski, H. 1978 Über Näherungsverfahren zur Lösung der nichtlinearen Schrödinger-Gleichung. *Math. Nachr.* **85**, 283–302.

Hasimoto, H. & Ono, H. 1972 Nonlinear modulation of gravity waves. *J. Phys. Soc. Japan* **33**, 805–811.

Johnson, R. S. 1977 On the modulation of water waves in the neighbourhood of $kh \approx 1{\cdot}363$. *Proc. R. Soc. Lond.* A **357**, 131–141.

Lake, B. M., Yuen, H. C., Rungaldier, H. & Ferguson, W. E. 1977 Nonlinear deep water waves: theory and experiment. Part 2. Evolution of a continuous wave train. *J. Fluid Mech.* **83**, 49–74.

Longuet-Higgins, M. S. 1980 Modulation of the amplitude of steep wind waves. *J. Fluid Mech.* **99**, 705–713.

Longuet-Higgins, M. S. & Stewart, R. W. 1962 Radiation stress and mass transport in gravity waves with application to 'surf beats'. *J. Fluid Mech.* **13**, 481–504.

LONGUET-HIGGINS, M. S. & STEWART, R. W. 1964 Radiation stresses in water waves; a physical discussion, with applications. *Deep-Sea Res.* **11**, 529–562.

MARTIN, D. U. & YUEN, H. C. 1980 Spreading of energy in solutions of the nonlinear Schrödinger equation. *Phys. Fluids* **23**, 1269–1271.

STOKES, G. G. 1849 On the theory of oscillatory waves. *Trans. Camb. Phil. Soc.* **8**, 441–455.

YUEN, H. C. & FERGUSON, W. E. 1978 Relationship between Benjamin–Feir instability and recurrence in the nonlinear Schrödinger equation. *Phys. Fluids* **21**, 1275–1278.